18TH WORLD CONFERENCE ON EARTHQUAKE ENGINEERING
WCEE2024
MILAN

MILAN, ITALY
30TH JUNE - 5TH JULY 2024

www.wcee2024.it

EXPERIMENTAL TEST ON A HYBRID INTER-MODULE CONNECTION FOR STEEL MODULAR BUILDING SYSTEMS

D.-A. Corfar[1] & K. D. Tsavdaridis[2]

[1] City, University of London, London, United Kingdom,

[2] City, University of London, London, United Kingdom, Konstantinos.Tsavdaridis@city.ac.uk

Abstract: *The context of the ongoing climate emergency has highlighted the pressing challenge of achieving a resilient and sustainable built environment. Steel modular building systems (MBSs) have gained a lot of traction due to noteworthy opportunities for disassembly and reuse harnessed by prefabrication, standardisation, and the use of demountable connections, yet research has shown that the seismic resilience of steel MBSs remains problematic. In this regard, the present study investigated the in-plane structural response to cyclic lateral loading of an inter-module joint (IMJ) prototype equipped with a hybrid inter-module connection (IMC) comprising of a high-damping rubber (HDR) bearing and a high-strength steel (HSS) bolt. The FEMA-SAC cyclic loading sequence was conducted in a quasi-static fashion on a meso-scale IMJ subassemblage to understand the effect of the HDR bearing on seismic performance of the joint under seismic action, by revealing its lateral load capacity, deformation modes, and energy dissipation capacity. The re-centring effect of the joint due to the HDR bearing was confirmed by the large recoverable displacement identified in the force-displacement, which came at the expense of higher EDC capacity. The IMJ prototype reached the end of the loading programme with 85% of the peak strength and limited plastic damage sustained by the frame members, meeting the qualifying drift angle capacity at strength degradation (θ_{SD} = 0.04 rad) for a special moment frame (SMF). Overall, it was shown that the hybrid IMC the hybrid IMC fulfilled its passive damage control role by delaying the full contribution of the IMJ frame members until large storey drift amplitudes were reached, effectively improving the reclaim and reuse opportunities in the event of an earthquake for the next-generation, sustainable and resilient steel MBSs.*

1 Introduction

In the context of the current climate emergency, steel Modular Building Systems (MBSs) have emerged as a sustainable modern method of construction (MMC) with compelling disassembly and reuse prospects (Gunawardena and Mendis, 2022; Nguyen *et al.*, 2023), yet natural hazards such as earthquakes can damage the structural frame beyond recovery without due consideration of structural resilience. Recent studies have emphasised the interdependence between sustainability and resilience in structural steel design (McConnell and Fahnestock, 2015; Fujita *et al.*, 2023; Grigorian, Sedighi and Mohammadi, 2023; Hao *et al.*, 2023), highlighting the increasing interest in damage control design principles. In line with the United Nations' Sustainable Development Goals (in particular Goals 9 and 11) (United Nations, Department of Economic and Social Affairs, 2015), it is worthwhile to further develop the technology of steel MBSs by mitigating the impact of extreme events on the functionality, repairability, demountability, and continued service of these structures.

The ever-increasing height of self-standing steel MBSs has drawn attention to the connections between modules (i.e., inter-module connections or IMCs) and the critical influence of their mechanical behaviour on the global structural response to lateral loads of sway modular structural systems (Lacey *et al.*, 2020; Farajian *et al.*, 2022; Wang and Tsavdaridis, 2022; Wang *et al.*, 2023). So far, studies have investigated the performance of IMCs based on capacity design criteria, in order to dissipate energy through the formation of plastic hinges in predetermined locations within the structural system. Although this method is effective in preventing collapse by controlling the global damage mechanism to some extent, the permanent damage sustained by sacrificial structural elements hinders functionality and retrofitting prospects (McCormick *et al.*, 2008).

In this regard, several review articles (Deng *et al.*, 2020; Chen *et al.*, 2021; Corfar and Tsavdaridis, 2022) have emphasised the potential of employing replaceable energy dissipating components in IMCs to enhance their mechanical response, yet accounts of this topic remain limited (Sultana and Youssef, 2018; Wu *et al.*, 2019; Jing *et al.*, 2021; Sendanayake *et al.*, 2021; Zhang, Xu and Li, 2022). In a recent paper (Corfar and Tsavdaridis, 2023), the authors have introduced a hybrid demountable IMC with high-damping rubber (HDR) and shape-memory alloy (SMA) components, and characterised the axial tension and combined compression and shear behaviours through validated finite element analysis (FEA). The proof-of-concept FEA study represents the first stage of the investigation, showcasing the cyclic performance of the connection at small-scale micro-level, yet further research is necessary in order to determine the large-scale, macro-level stress evolution and force-transfer mechanisms between the interfaces of modular structural systems equipped with the hybrid IMC.

Hence, this paper presents the second stage of the investigation, which aims to study the in-plane structural response to cyclic lateral loading of an inter-module joint (IMJ) prototype equipped with a hybrid inter-module connection (IMC) comprising of a high-damping rubber (HDR) bearing and a high-strength steel (HSS) bolt. The experimental test has been carried out on a meso-scale joint sub-assemblage made of full-scale structural members to avoid potential issues pertaining to scaling effects. The IMJ prototype has been subjected to cyclic lateral loading using the standard FEMA-SAC loading sequence to reveal its aseismic behaviour and understand the effect of the HDR bearing on a bolted inter-module connection, as well as the contribution of the hybrid IMC to the overall structural performance of the IMJ assembly.

2 The hybrid inter-module connection

The assembly illustrated in Figure 1 represents a corner IMJ assembled with a laminated elastomeric bearing (LEB) as a core clamped between the steel box corner fittings of volumetric modules by means of a bolt assembly. The connection has been designed to fulfil the essential functions of vertical and horizontal connectivity between modules. Axial compression is transferred between the corner posts through the laminated elastomeric bearing made with steel reinforcing plates to control the level of vertical displacement, whereas tensile axial force is resisted by the bolt assembly. Horizontal shear forces are transferred through a combined mechanism of friction between the faying steel surfaces and the superposition of shear resistances of the rubber layers and bolt rod, while the interlocking pins prevent accidental sliding.

To improve the energy dissipation capacity of the connection, the bearing has been fabricated with filled (high-damping) rubber instead of low-damping (unfilled) rubber, as the presence of high percentages of carbon black filler in HDR results in a much more pronounced hysteresis at the lower working shear strain levels (in the range of 50%-100%) due to the breakdown of carbon filler chain networks (Lindley and Gough, 2015). By comparison, unfilled (low-damping) rubber typically exhibits hysteresis due to strain-crystallisation at extensions greater than 200% strain. Moreover, filled (high-damping) rubber presents a higher initial shear stiffness, ensuring that the IMC is not easily excited during more frequent low-magnitude earthquakes or common low-intensity wind loads, reserving the available supplemental damping for stronger lateral loads.

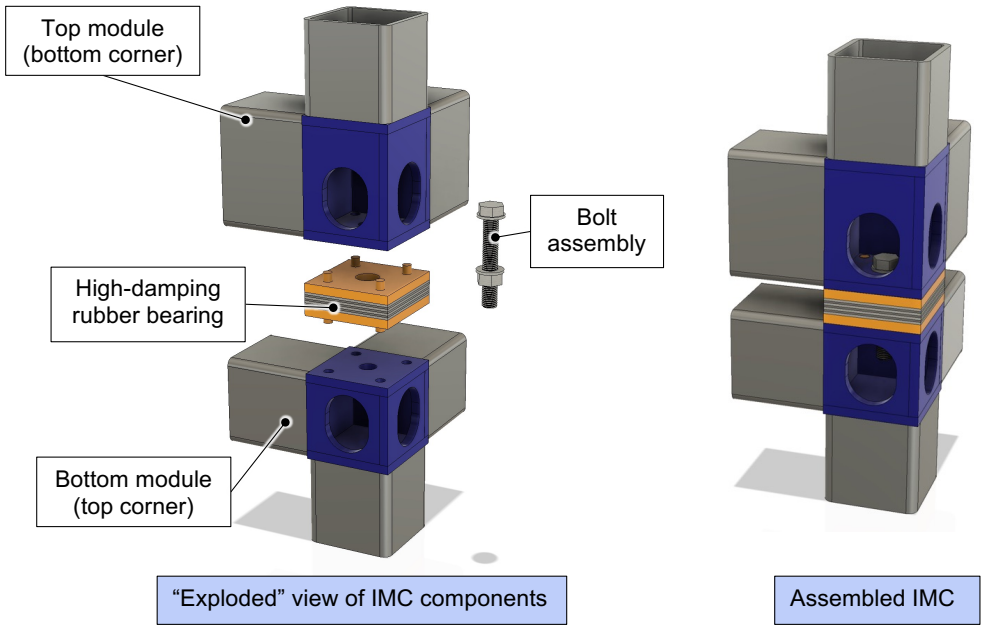

Figure 1. Configuration of the hybrid inter-module connection.

3 Experimental programme

3.1 Details of the meso-scale test arrangement

The meso-scale inter-module joint (IMJ) prototypes (Figure 2) are based on the beam-column subassemblage with column loading (J/C) recommended by Lacey et al. (2022). The IMJ prototype consists of top and bottom steel beam-column (BC) subassemblages connected by means of the hybrid inter-module connection (IMC). The choice for this type of frame has been attributed to its ability to realistically replicate the anticipated points of inflection in the deformed shape of unbraced modular frames subjected to earthquake loading, including the contribution of the connecting framing members and that of the beam-to-column joint (BCJ).

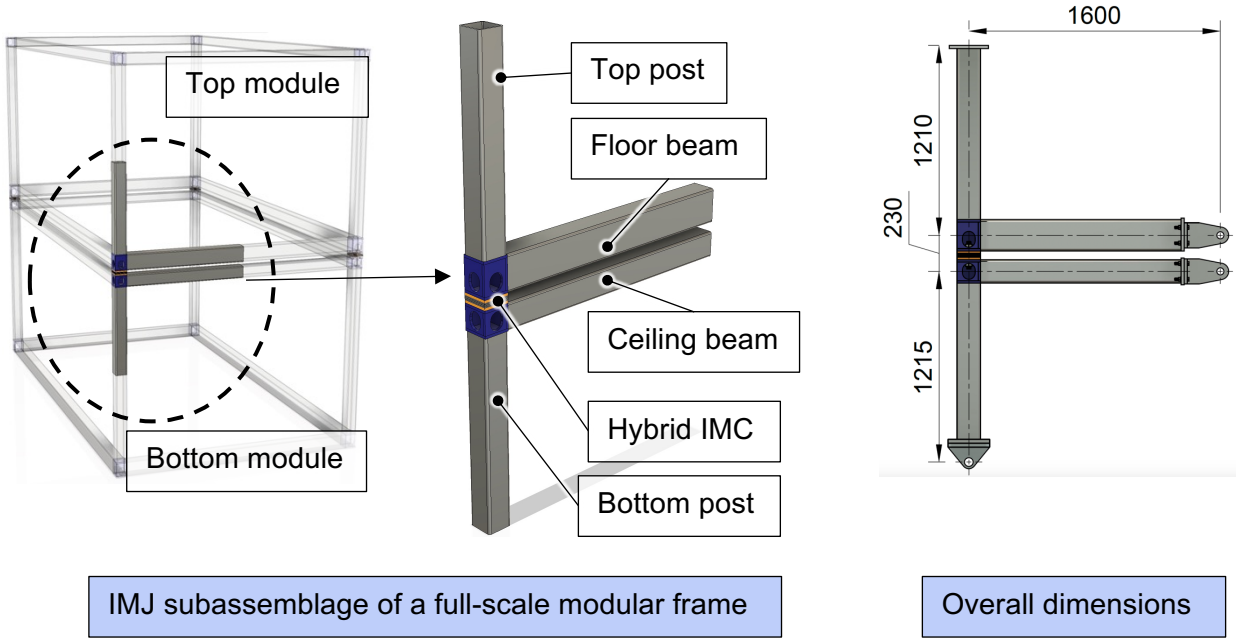

Figure 2. Schematic of meso-scale IMJ prototype

3.2 Dimensions and material properties of the IMJ prototype components

Steel beam-column sub-assemblages

The beam-column (BC) frames are made of standard hollow sections joined to box corner fittings by complete joint penetration (CJP) groove welds, while cap plates are attached to each member's end through all around fillet welds. The role of the endplates is to help realise the bolted connections between the samples and test rig. The box corner fittings have been fabricated from 15-mm-thick steel plates joined together by CJP groove welding. Detailed drawings of the steel frames are illustrated in Figure 3, while material properties of the frame members based on mill test certificates are provided in Table 1.

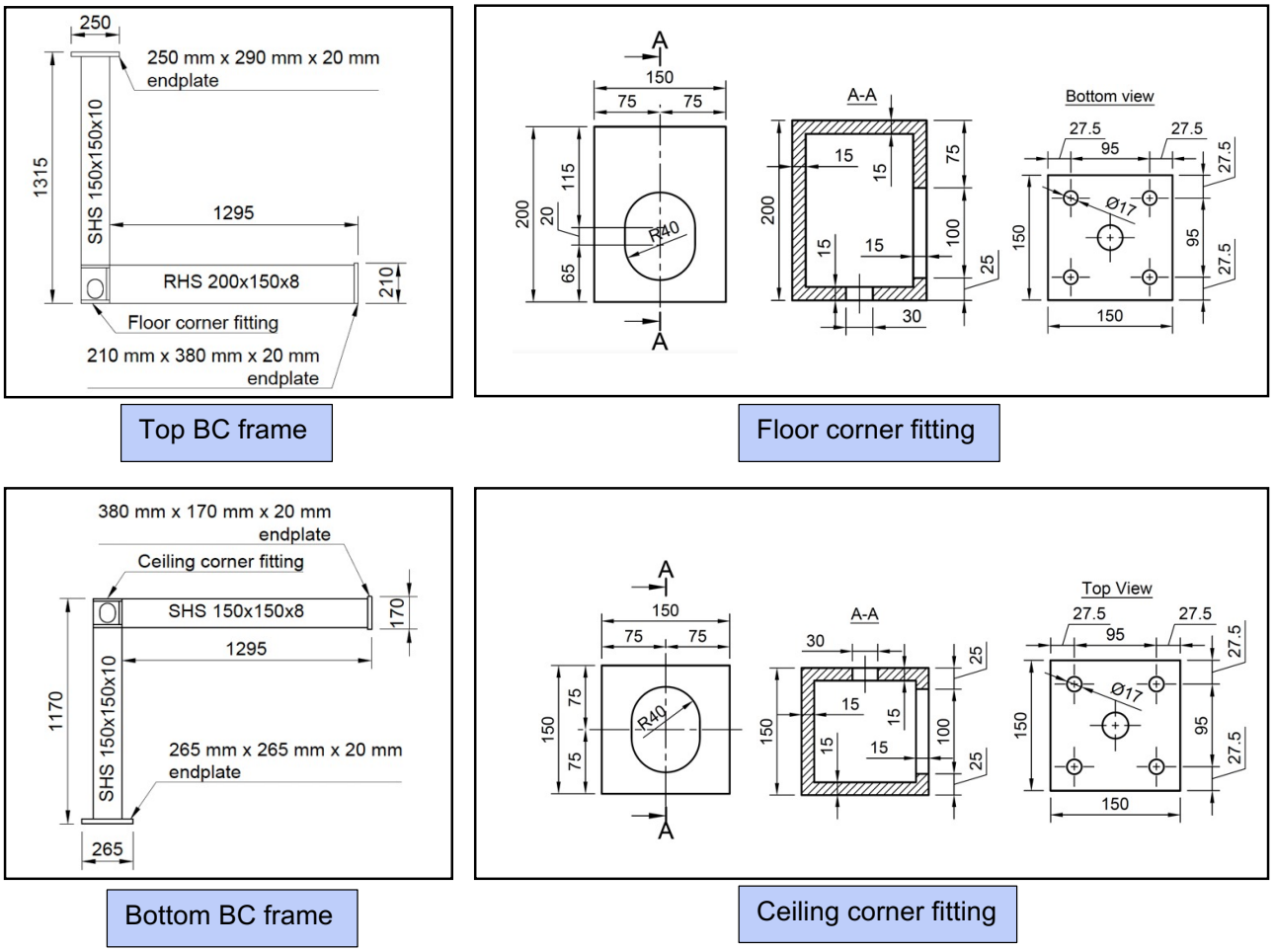

Figure 3. Details of the steel beam-column frames (units: millimetres).

Table 1. Material properties of steel

Frame element	Sectional properties (mm x mm x mm)	Steel grade	Yield Strength (N/mm^2)	Ultimate Strength (N/mm^2)	Elongation (%)
Top and bottom posts	150 x 150 x 10	S355J2H	367	514	30
Ceiling beam	150 x 150 x 8	S355J2H	506	539	33.4
Floor beam	150 x 200 x 8	S355J2H	363	519	29

High-damping rubber core

The laminated elastomeric bearing has been fabricated using a proprietary high damping rubber (HDR) compound. Double-bonded shear (DBS) testing has been carried out to characterise the material properties of the rubber. Sinusoidal waveforms of 0.5 Hz frequency at ±1, ±2, ±5, ±10, ±20, ±50, ±100, ±150, ±200 % shear strains have been applied to the test pieces at a constant temperature of 23 +/-2 °C. Six cycles have been performed at each strain amplitude to capture the stress-softening behaviour (Mullins effect (Mullins, 1969)) typically exhibited in rubber during cyclic loading at a constant amplitude. As the Mullins effect is most

pronounced during the first two cycles and becomes negligible after six-to-ten cycles (Burtscher and Dorfmann, 2004), the data extracted for material characterisation is taken from the sixth loading cycle. Figure 4 (a) shows the results for the cyclic DBS test used to determine the representative material properties listed in Table 2. The highly nonlinear load-deflection behaviour characteristic for HDR is unmistakeable. The shear modulus, G, the effective shear stiffness, $k_{eff.b}$, and the effective damping ratio, $\xi_{eff.b}$, have been determined as per EN 15129 (BSI, 2018) using equations (1) – (3), where τ_{max} is the maximum nominal shear stress, γ_{max} is the maximum nominal shear strain, F^+ and F^- are the maximum and minimum shear force values in the chosen cycle with d^+ and d^- as the corresponding displacements, and H is the energy dissipated per cycle.

$$G = \tau_{max}/\gamma_{max} \quad (1)$$

$$k_{eff.b} = (F^+ - F^-)/(d^+ - d^-) \quad (2)$$

$$\xi_{eff.b} = \frac{2H}{\pi k_{eff.b}(d^+ - d^-)^2} \quad (3)$$

Table 2. Mechanical properties of the high damping rubber

Property	**Value**
Hardness[a] (IRHD[b])	86
Shear modulus, G[c] (MPa)	0.61
Effective damping ratio, $\xi_{eff.b}$[c] (%)	18.46

[a] based on shear modulus at 5% shear strain
[b] International rubber hardness degree
[c] at 100% shear strain

The variation of shear stiffness and damping properties of the HDR with strain amplitude is provided in Figure 4 (b). It can be seen that the shear modulus assumes values between 16.97 MPa and 0.44 MPa, falling abruptly for strains up to 10% and stabilising after about 50% shear strain. This is in good agreement with the well-known phenomenon of decreasing modulus with increasing deformation due to the breakage of weak filler clusters within the filled rubber's microstructure, known as the Payne effect (Payne, 1962). On the other hand, the effective damping ratio's dependence on the shear strain magnitude is a lot less prominent, ranging between 17.22% and 22.06% for the strain range considered herein.

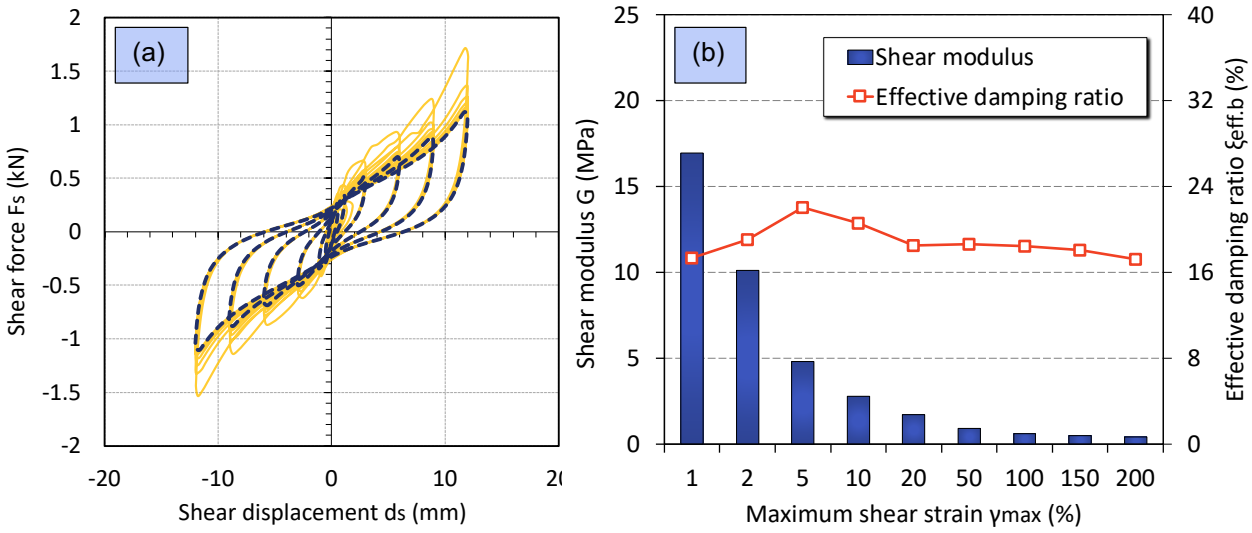

Figure 4. Results of the DBS tests: (a) hysteretic curves with sixth cycle highlighted, (b) variation of secant shear modulus and equivalent viscous damping ratio with strain amplitude.

To fabricate the bearing, steel shims and rubber sheets have been alternated in a custom mould, where the rubber vulcanisation (curing) and bonding between rubber and metal surfaces occur simultaneously at elevated temperatures under pressure (Lindley and Gough, 2015). For the rubber to metal bonding process, a primer layer and proprietary bonding adhesive are applied to the degreased and sand-blasted surfaces of the steel plates. During vulcanisation, strong crosslinks are formed between the molecules of the viscous liquid elastomer, turning the compound into the solid polymer with high elasticity and strength required for engineering applications (Gent, 2012).

The bearing consists of two outer steel plates (150 mm x 150 mm x 15 mm), four rubber layers (150 mm x 150 mm x 4 mm) and three steel shims (150 mm x 150 mm x 3 mm), designed to achieve a shape factor of S = 8.85 to limit the vertical displacement. A central hole (40 mm diameter) has been cut through the plates to accommodate the bolt assembly. The hole diameter was purposefully made larger than the hole diameter in the corner fittings to ensure that the bolt does not interfere with the inner surface of the bearing during the lateral cyclic loading imposed on the IMJ prototype. Blind holes (15 mm diameter x 10 mm deep) have been milled on one side of the outer plates to push-fit the four cylindrical steel lugs. Loctite has been used to ensure the lugs on the bottom surface do not detach and fall during transportation and testing. The design details of the fabricated bearings are presented in Figure 5.

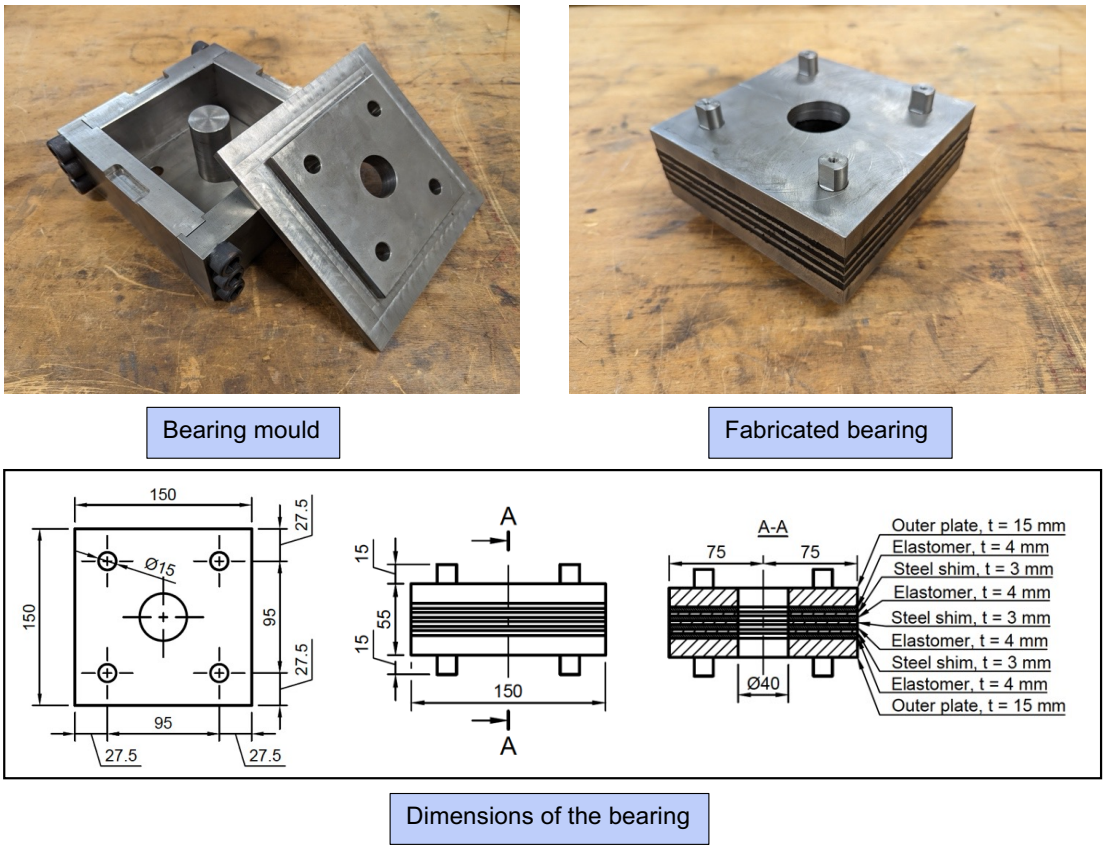

Figure 5. Details of the HDR core (units: millimetres).

Bolt assembly

A standard M24 x 150mm full-thread hexagon head bolt made of class 8.8 high-strength steel has been used to connect the box corner fittings. The choice for a typical structural bolt has facilitated the focus of the present research on the effect of the rubber bearing over the mechanical behaviour of the tested IMJ prototype.

3.3 Details of the test apparatus and loading sequence

The test rig illustrated in Figure 6 has been designed to accommodate the bi-axial loading of the IMJ sub-assemblage. A test commences with the application of a force-controlled compressive axial load of 100 kN over 1 minute through the vertical hydraulic jack to simulate the gravitational load from the self-weight of upper

building levels. Based on a realistic on-site installation scenario of a modular building, a snug-tight condition is achieved in the hybrid IMC before initiating the axial load step. The axial load is then maintained for 10 minutes to account for the potential loss of bolt pre-tension due the compression set in the rubber bearing. The applied axial load is equivalent to ca. 5% of the compressive yield capacity of the column's cross-section, $N_{c.Rd}$, as defined in Eurocode 3, Part 1 (BSI, 2015) for members not susceptible to local buckling failure. The axial load is maintained during subsequent test stages, while the sample is subjected to cyclic lateral load using the horizontal actuators. Following the prequalification and cyclic qualification testing provisions as per ANSI/AISC 341-22 (AISC, 2022), the displacement-controlled standard FEMA/SAC loading sequence (SAC Joint Venture, 2000) given in Table 3 has been adopted in a quasi-static cyclic fashion at a rate of 10mm/min. The equivalent horizontal displacement applied at the top of the column, Δ_h, has been determined based on the storey drift angle (also known as chord rotation), θ (rad) using equation (4). Due to constructional limitations, the maximum lateral drift level that could be accommodated by the test rig was that of θ = □ 0.04 rad.

$$\theta = \Delta_h / H_{storey} \tag{4}$$

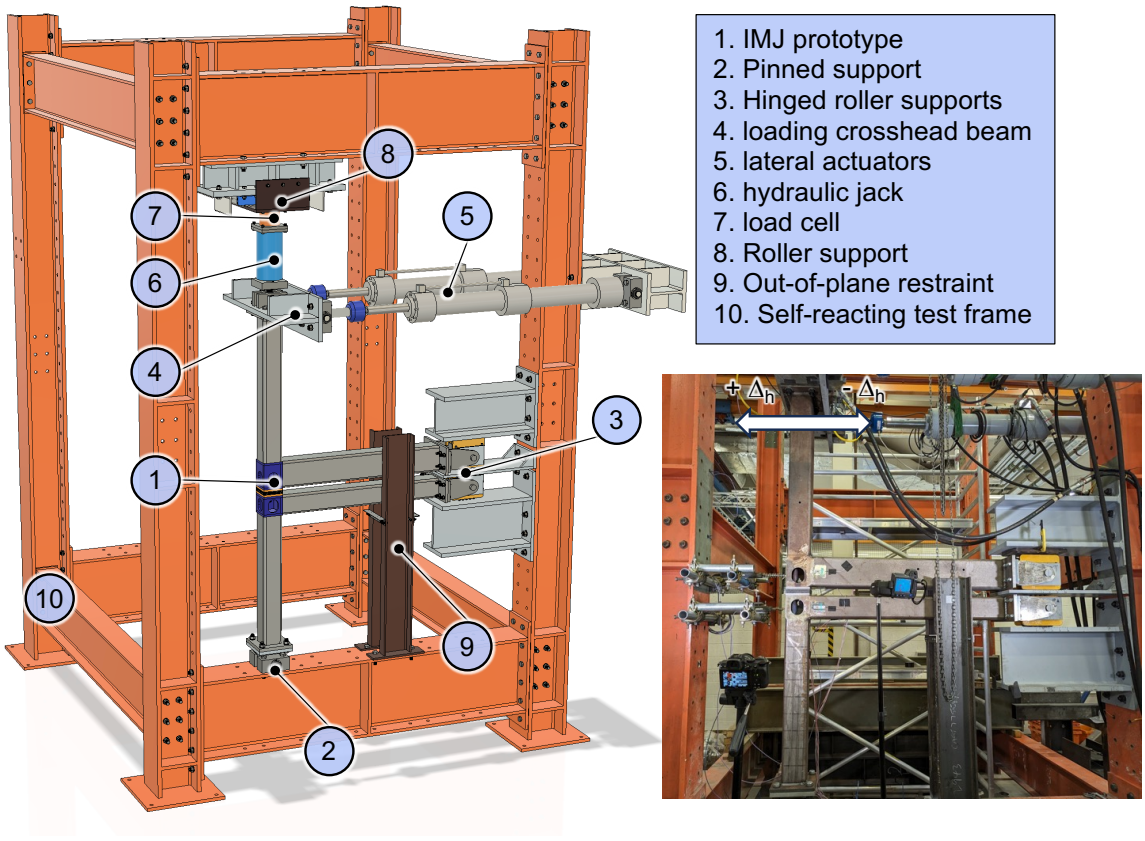

Figure 6. Schematic of the IMJ prototype and its loading system

Table 3. Loading sequence

Load step	Story drift angle, θ (rad)	Equivalent lateral displacement, Δ_h (mm)	Number of cycles
1	0.00375	10.3125	6
2	0.005	13.75	6
3	0.0075	20.625	6
4	0.01	27.5	4
5	0.015	41.25	2
6	0.02	55	2
7	0.03	82.5	2
8	0.04	110	2

3.4 Instrumentation layout

The in-plane lateral displacement applied at the top of the sample is recorded by the built-in linear variable displacement transformers (LVDTs) of the servo-hydraulic actuators (T05) and is used to obtain the load-displacement hysteresis loops. Two linear potentiometers (T01-02) have been arranged horizontally along the centrelines of the floor and ceiling beams to record the relative displacement between the floor and the ceiling beams. Additionally, two vertical potentiometers have been installed between the floor and ceiling corner fittings (T03) and at the top jack (T04) to measure the vertical displacement of the rubber bearing and the total vertical displacement of the specimen respectively. A total of 10 strain gauges have been installed on the beam and posts near the BCJ zone to monitor the evolution of strains in the regions expected to develop the highest stress levels. Details of the arrangement of potentiometers and the locations of strain gauges are illustrated in Figure 7.

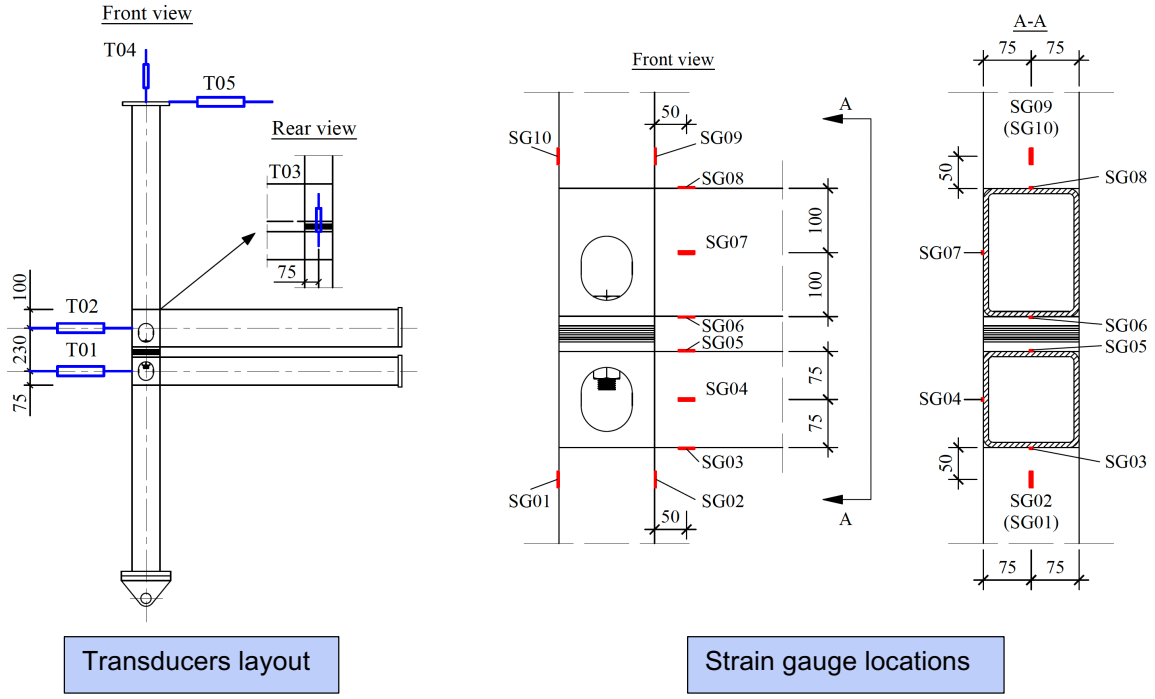

Figure 7. Instrumentation plan

4 Results of the experimental tests

4.1 Hysteretic performance

At the end of the 10 minute wait step with 100 kN applied vertical load on the IMJ test frame, the linear potentiometer T03 recorded a compressive set in the rubber bearing of -0.54 mm. This effect generated a partial loss of tension in the original snug-tight condition of the bolt assembly, preventing the full involvement of the bolt at small horizontal displacements. As the quasi-static cyclic loading sequence commenced, the 3 mm bolt hole clearance cumulated with the partially loose condition of the bolt assembly ensured that the initial non-linear force-displacement relationship was almost entirely due to the shear behaviour of the rubber bearing, characterised by a high initial stiffness with quick softening followed by increased stiffness at larger strains.

The graph of the applied lateral load versus the displacement at the tip of the top post recorded during the quasi-static cyclic loading test is plotted in Figure 8 (a). An initial qualitative appraisal of the hysteretic loop reveals a stable performance, with no obvious signs of strength or stiffness degradation and a pronounced S-shaped path during the small-deformation cycles, typical for filled rubber under shear loading conditions. The curve shows very limited residual displacement up to 3% story drift angle, attributed to the re-centring capability of the rubber bearing, while the increasing permanent displacement at 4% story drift angle indicates the onset of a more significant contribution of the steel frame members and the BC joints to the overall response of the IMJ to cyclic lateral loading. The rubber bearing's effective re-centring effect (represented by 68% recoverable displacement in the positive loading direction and 55% recoverable displacement in the negative loading

direction) has come at the expense of a fat loop like those exhibited by metallic yielding-based systems, suggesting that the hysteresis demonstrated by the hybrid IMJ is mostly a result of the work done by the high-damping rubber bearing during the cyclic shear straining.

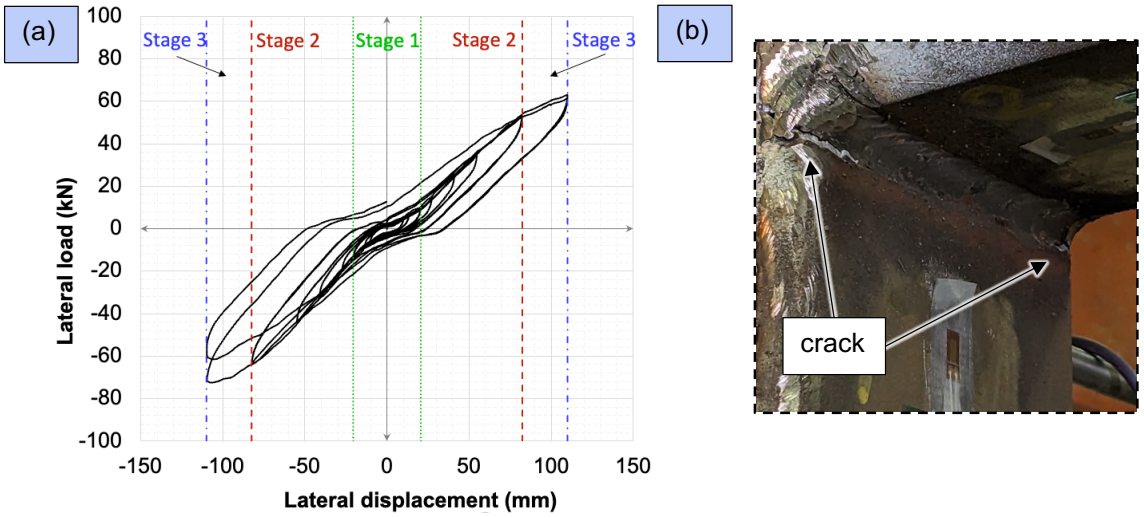

Figure 8. Hysteretic curve (a) and weld crack at the ceiling BC joint (b)

The structural behaviour of the IMJ prototype has been characterised by three main force-displacement stages, each identifiable by a change in stiffness attributed to events observed during the test. During Stage 1 (0 mm to □20.625 mm lateral displacement), the IMJ prototype displayed a lower stiffness as lateral load was mostly resisted by a combination of the friction between the box corner endplates and rubber bearing outer plates, the shear stiffness of the rubber and slipping of the bolt assembly. As the IMJ prototype entered Stage 2 (limited by □82.5 mm lateral displacement), the bolt rod experienced a combined shear-bending action as it was fully engaged between the top and bottom box corner plates leading to an increased overall stiffness of the IMJ prototype due to the additional contribution of the flexural stiffness of its members. The third and final stage displayed a lower stiffness, explained by the increasing bending deformation of the bolt rod which allows further extension to occur in the rubber layers of the bearing. Overall, the IMJ prototype displayed stiffer behaviour in the negative loading direction due to the contribution of the intra-module connections represented by the rigid beam-to-column joints which stiffened that side of the assembly. The values of the lateral load capacity (P_i), lateral load displacement (d_i), and stiffness (k_i) representative for each stage have been reported in Table 4, using data from the first cycle of the respective load step.

Table 4. Mechanical parameters of the IMJ prototype

Load direction	P_1 (kN)	d_1 (mm)	k_1 (kN/mm)	P_2 (kN)	d_2 (mm)	k_2 (kN/mm)	P_3 (kN)	d_3 (mm)	k_3 (kN/mm)
(+)	10.2	20.6	0.49	50.9	81.9	0.66	63.1	110.0	0.44
(-)	-14.2	-20.7	0.68	-63.8	-82.4	0.80	-71.2	-109.7	0.27

At the end of the test, an evident loss of strength was noticed during the reverse loading in the 2nd cycle of □ 110 mm lateral displacement (4% story drift angle) as the peak lateral load (P_{max} = -61.6 kN) reached approximately 85% of the peak lateral load (P_{max} = -72.5 kN) previously recorded during the first cycle of the same amplitude, and the onset of cracking of the fillet welds was observed at the inside corner of the ceiling BC joint (Figure 8 (b)). This type of failure was in good agreement with that reported by Chen et al. (2017) for similar one-sided IMJ frames with unstiffened BC joints subjected to quasi-static cyclic loading, emphasizing once more the critical role of the BC joints and the importance of weld quality at these highly-stressed regions. Despite this initiation of strength degradation, the state of the specimen did not hinder its stability under gravity load, such that it was possible to reach the end of the 2nd □ 4 % storey drift cycle, marking the end of the loading programme that could be accommodated by the test rig. After the test, the plastic deformation of the bolt rod was limited such that it was possible to undo the nut with a regular spanner to disassemble the joint assembly. According to acceptance criteria as defined in FEMA 350 (SAC Joint Venture, 2000), the IMJ prototype met the minimum qualifying drift angle capacity for both strength degradation (θ_{SD} = 0.02 rad) and

connection failure (θ_u = 0.03) for an ordinary moment frame (OMF), while also meeting the qualifying drift angle capacity at strength degradation (θ_{SD} = 0.04 rad) for a special moment frame (SMF).

4.2 Deformation patterns and strain evolution

Using the readings from transducers T01, T02, and T05, the deformation modes along the height of the test frame have been constructed in Figure 10, based on data from the first cycle at each storey drift amplitude. Because of operational issues with the linear potentiometers during the test, data was not available for the negative loading direction corresponding to the 0.04 rad storey drift step. The gradients of the lateral displacement along the height of the frame indicate a comparable contribution between the top and bottom posts, while most of the inter-storey drift is concentrated in the IMC region. The stiffer behaviour in the negative loading direction was exposed again, while the locking effect of the bolt assembly throughout the second stage of the force-displacement curve was also highlighted by the constant relative displacement of the connected box corners up to the level of 2% story drift angle.

The strain gauge data revealed that the steel members of the IMJ prototype worked within the elastic state of deformation the whole time during the 0 to □0.03 rad storey drift angle load steps, while the onset of steel yielding was reached in the top flange of the top beam (SG08), and inside flanges of the posts (SG02 and SG09) only during the negative loading direction of the first □0.04 rad cycle. Yield strain was determined using the yield strength values reported in Table 1 assuming a Young's modulus of 210,000 MPa. These results suggest that the hybrid IMC made of a high-damping rubber bearing and high-strength steel bolt is effective in its passive damage control function by resisting most of the lateral load up to □0.03 rad storey drift angle, while the stress in the main framing members is kept below yielding levels until θ = □0.04 rad has been reached.

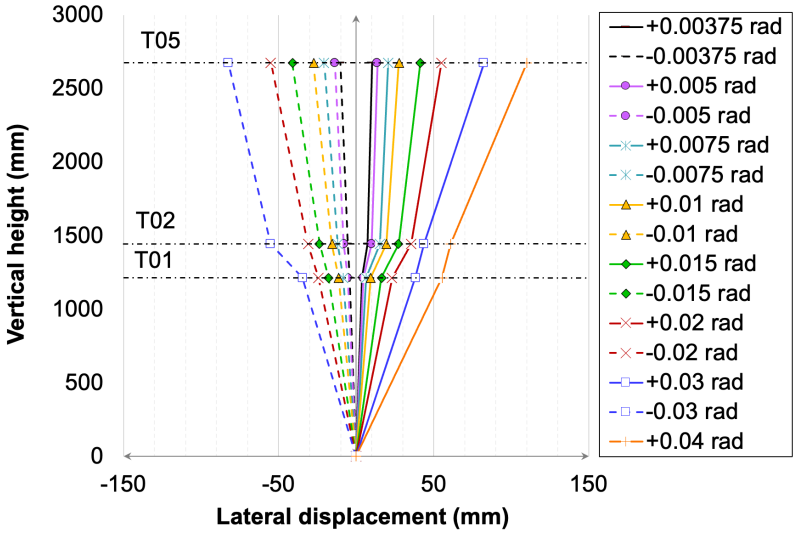

Figure 10. Deformation pattern of the IMJ prototype.

4.3 Energy dissipation capacity

The energy dissipation capacity (EDC) was evaluated by the equivalent viscous damping coefficient (Chopra, 2020), which accounts for all energy dissipating mechanisms present during the cyclic loading. Based on data points from the last hysteresis loop during the 2nd cycle of θ = □0.04 rad, the resulting equivalent damping coefficient of 0.12 was lower than the values obtained by similar tested specimens by Chen et al. (2017) at comparable levels of applied lateral displacement. While a more ductile bolt may improve the low EDC predicted also by the shape of the hysteresis loop, the limited permanent deformations exhibited by frame members together with the pronounced re-centring effect remain as evidence for the favourable effect of the hybrid IMC with a HDR bearing and HSS bolt on the seismic resilience of the IMJ prototype.

5 Concluding remarks

The present study has been concerned with the experimental test of an inter-module joint prototype comprising a high-damping rubber bearing connected between the box corner fittings of top and bottom subassemblages by means of a high-strength steel bolt. The test represented the second stage in the development of the hybrid

IMC developed by the authors, in which the IMJ prototype was subjected to the full FEMA-SAC cyclic loading sequence in a quasi-static fashion to better understand the effect of the high-damping rubber bearing on the seismic performance of the joint.

The force-displacement hysteretic loop confirmed the presence of a good re-centring ability of the joint due to the recoverable deformation of the HDR bearing. Based on a hybrid working mechanism defined by the HDR shear straining and combined shear-bending deformation of the HSS bolt, the hybrid IMC fulfilled its passive damage control role by delaying the full contribution of the IMJ frame members until large storey drift amplitudes were reached.

While the onset of cracking was observed near the weld at the ceiling BC connection, the IMJ prototype reached the end of the quasi-static cyclic loading protocol (2nd cycle of 0.04 rad storey drift angle) with 85% of its peak strength and limited damage suffered by the main framing members emphasizing the resilience of the connection system. In the future, stiffened BC connections should be adopted to improve the lateral load capacity and avoid weld cracking during the last loading step, while means of enhancing the joint's EDC without compromising on the re-centring effect and low-damage state of the frame members should be investigated.

6 References

AISC (2022) *Seismic Provisions for Structural Steel Buildings*. Chicago: American Institute of Steel Construction. Available at: https://www.aisc.org/publications/steel-standards/aisc-341/.

BSI (2015) *Eurocode 3: Design of steel structures - Part 1-1: General rules and rules for buildings*. London: BSI.

BSI (2018) *Anti-seismic devices*. London: BSI.

Burtscher, S.L. and Dorfmann, A. (2004) 'Compression and shear tests of anisotropic high damping rubber bearings', *Engineering Structures*, 26(13), pp. 1979–1991. Available at: https://doi.org/10.1016/j.engstruct.2004.07.014.

Chen, Z. *et al.* (2017) 'Experimental study of an innovative modular steel building connection', *Journal of Constructional Steel Research*, 139, pp. 69–82. Available at: https://doi.org/10.1016/j.jcsr.2017.09.008.

Chen, Z. *et al.* (2021) 'Exploration of the multidirectional stability and response of prefabricated volumetric modular steel structures', *Journal of Constructional Steel Research*, 184. Available at: https://doi.org/10.1016/j.jcsr.2021.106826.

Chopra, A.K. (2020) *Dynamics of Structures: Theory and Applications to Earthquake Engineering*. 5th edn. Harlow: Pearson.

Corfar, D.-A. and Tsavdaridis, K.D. (2022) 'A comprehensive review and classification of inter-module connections for hot-rolled steel modular building systems', *Journal of Building Engineering*, 50, p. 104006. Available at: https://doi.org/10.1016/j.jobe.2022.104006.

Corfar, D.-A. and Tsavdaridis, K.D. (2023) 'A hybrid inter-module connection for steel modular building systems with SMA and high-damping rubber components', *Engineering Structures*, 289, p. 116281. Available at: https://doi.org/10.1016/j.engstruct.2023.116281.

Deng, E.-F. *et al.* (2020) 'Seismic performance of mid-to-high rise modular steel construction - A critical review', *Thin-Walled Structures*, 155, p. 106924. Available at: https://doi.org/10.1016/j.tws.2020.106924.

Farajian, M. *et al.* (2022) 'Classification of inter-modular connections for stiffness and strength in sway corner-supported steel modular frames', *Journal of Constructional Steel Research*, 197, p. 107458. Available at: https://doi.org/10.1016/j.jcsr.2022.107458.

Fujita, M. *et al.* (2023) 'Japanese Efforts to Promote Steel Reuse in Building Construction', *Journal of Structural Engineering*, 149(1), p. 04022225. Available at: https://doi.org/10.1061/(ASCE)ST.1943-541X.0003473.

Gent, A.N. (2012) *Engineering with Rubber: How to Design Rubber Components*. 3rd edn. München: Hanser.

Grigorian, M., Sedighi, S. and Mohammadi, H. (2023) 'Plastic design of sustainable steel earthquake resistant structures', *Engineering Structures*, 289, p. 116178. Available at: https://doi.org/10.1016/j.engstruct.2023.116178.

Gunawardena, T. and Mendis, P. (2022) 'Prefabricated Building Systems—Design and Construction', *Encyclopedia*, 2(1), pp. 70–95. Available at: https://doi.org/10.3390/encyclopedia2010006.

Hao, H. *et al.* (2023) 'Towards next generation design of sustainable, durable, multi-hazard resistant, resilient, and smart civil engineering structures', *Engineering Structures*, 277, p. 115477. Available at: https://doi.org/10.1016/j.engstruct.2022.115477.

Jing, J. *et al.* (2021) 'Seismic protection of modular buildings with galvanised steel wall tracks and bonded rubber units: Experimental and numerical study', *Thin-Walled Structures*, 162. Available at: https://doi.org/10.1016/j.tws.2021.107563.

Lacey, A.W. *et al.* (2020) 'Effect of inter-module connection stiffness on structural response of a modular steel building subjected to wind and earthquake load', *Engineering Structures*, 213. Available at: https://doi.org/10.1016/j.engstruct.2020.110628.

Lindley, P.B. and Gough, J. (2015) *Engineering Design with Natural Rubber*. 6th edn. Bertford: Tun Abdul Razak Research Centre.

McConnell, J.R. and Fahnestock, L.A. (2015) 'Innovations in Steel Design: Research Needs for Global Sustainability', *Journal of Structural Engineering*, 141(2), p. 02514001. Available at: https://doi.org/10.1061/(ASCE)ST.1943-541X.0001185.

McCormick, J. *et al.* (2008) 'Permissible Residual Deformation Levels For Building Structures Considering Both Safety And Human Elements', in. *The 14th World Conference on Earthquake Engineering*.

Mullins, L. (1969) 'Softening of Rubber by Deformation', *Rubber Chemistry and Technology*, 42(1), pp. 339–362. Available at: https://doi.org/10.5254/1.3539210.

Nguyen, T.D.H.N. *et al.* (2023) 'An innovative approach to temporary educational facilities: A case study of relocatable modular school in South Korea', *Journal of Building Engineering*, 76, p. 107097. Available at: https://doi.org/10.1016/j.jobe.2023.107097.

Payne, A.R. (1962) 'The dynamic properties of carbon black-loaded natural rubber vulcanizates. Part I', *Journal of Applied Polymer Science*, 6(19), pp. 57–63. Available at: https://doi.org/10.1002/app.1962.070061906.

SAC Joint Venture (2000) *Recommended Seismic Design Criteria for New Steel Moment-Frame Buildings*. Federal Emergency Management Agency.

Sendanayake, S.V. *et al.* (2021) 'Enhancing the lateral performance of modular buildings through innovative inter-modular connections', *Structures*, 29, pp. 167–184. Available at: https://doi.org/10.1016/j.istruc.2020.10.047.

Sultana, P. and Youssef, M.A. (2018) 'Seismic Performance of Modular Steel-Braced Frames Utilizing Superelastic Shape Memory Alloy Bolts in the Vertical Module Connections', *Journal of Earthquake Engineering*, 24(4), pp. 628–652. Available at: https://doi.org/10.1080/13632469.2018.1453394.

United Nations, Department of Economic and Social Affairs (2015) *Transforming our World: The 2030 Agenda for Sustainable Development*. A/RES/70/1. United Nations. Available at: https://sdgs.un.org/2030agenda (Accessed: 8 June 2023).

Wang, Z. *et al.* (2023) 'Automated minimum-weight sizing design framework for tall self-standing modular buildings subjected to multiple performance constraints under static and dynamic wind loads', *Engineering Structures*, 286, p. 116121. Available at: https://doi.org/10.1016/j.engstruct.2023.116121.

Wang, Z. and Tsavdaridis, K.D. (2022) 'Optimality criteria-based minimum-weight design method for modular building systems subjected to generalised stiffness constraints: A comparative study', *Engineering Structures*, 251, p. 113472. Available at: https://doi.org/10.1016/j.engstruct.2021.113472.

Wu, C.X. *et al.* (2019) 'Research on seismic behaviour analysis of shock absorbing structure and connecting joints of container assembly structures', *Steel Construction*, 34(4), pp. 1-8+73.

Zhang, G., Xu, L.-H. and Li, Z.-X. (2022) 'Experimental evaluation on seismic performance of a novel plug-in modular steel structure connection system', *Engineering Structures*, 273, p. 115099. Available at: https://doi.org/10.1016/j.engstruct.2022.115099.